MICROSTRUCTURAL SENSITIVE FATIGUE MODELING OF ADDITIVELY MANUFACTURED TI-6AL-4V

Amanda J. Sterling, Brian Torries, Nima Shamsaei*, Scott M. Thompson, Steven R. Daniewicz

Department of Mechanical Engineering, Mississippi State University, MS 39762
Center for Advanced Vehicular Systems (CAVS), Mississippi State University, MS 39762
REVIEWED
*Corresponding author:
Email: shamsaei@me.msstate.edu
Phone: (662) 325 2364

Abstract

A common issue in powder-based Additive Manufacturing (AM) techniques is porosity. While process parameters can be controlled to limit this occurrence, complete elimination without post-processing is difficult. Because porosity can significantly affect fatigue behavior of AM parts, it is important to understand and model this material trait. In this study, the porosity in various Ti-6Al-4V specimens fabricated via Laser Engineered Net Shaping (LENS) was determined prior to fatigue testing. Void distribution and morphology was quantified. Fractography was performed to determine the specimen's transition through crack initiation and propagation stages. These results were used to calibrate a microstructure-sensitive fatigue model for predicting the fatigue behavior of as-built and heat treated LENS Ti-6Al-4V.

Introduction

Additive manufacturing (AM) is a manufacturing technique that allows for the fabrication of a part through the repetitious deposition of material layers. This process allows for the creation of complex geometries and even functionally-graded materials. Laser-based powder methods, such as blown powder or powder bed, are commonly employed for AM of metals, such as Laser Engineered Net Shaping (LENS) or Selective Laser Melting (SLM), respectively. While additive processes such as LENS have the ability to fabricate complex geometries that are unobtainable through traditional manufacturing techniques, they are still prone to generating defects, such as porosity, in built parts. For instance, pores can occur due to gas being trapped in the melt pool during deposition. Other process defects include un-melted powder (i.e. inclusions) or lack of fusion between layers. All of these, when present in a part, can alter its mechanical and fatigue properties.

The highly localized/transient thermal histories and time-dependent cooling rates resulting from AM processes such as LENS can lead to unique microstructures [1-5]. When the AM method utilizes process parameters that do not change with time (or with layer) these effects can become exaggerated. For example, large columnar grains can form within LENS Ti-6Al-4V [1], in contrast to the equiaxed grains typically found in wrought Ti-6Al-4V. Process parameters can be altered prior or during LENS to control local cooling rates for achieving target density and part quality. However, the occurrence of process defects, combined with typically-anisotropic microstructural features, results in DLD/LENS parts having different mechanical properties and fatigue behavior.

As shown in Figure 1, the fatigue curves for wrought and LENS Ti-6Al-4V (heat treated and as-built) are notably different [6]. It is clear that there is a need for a microstructure-sensitive model for more accurately predicting the mechanical performance of AM parts.

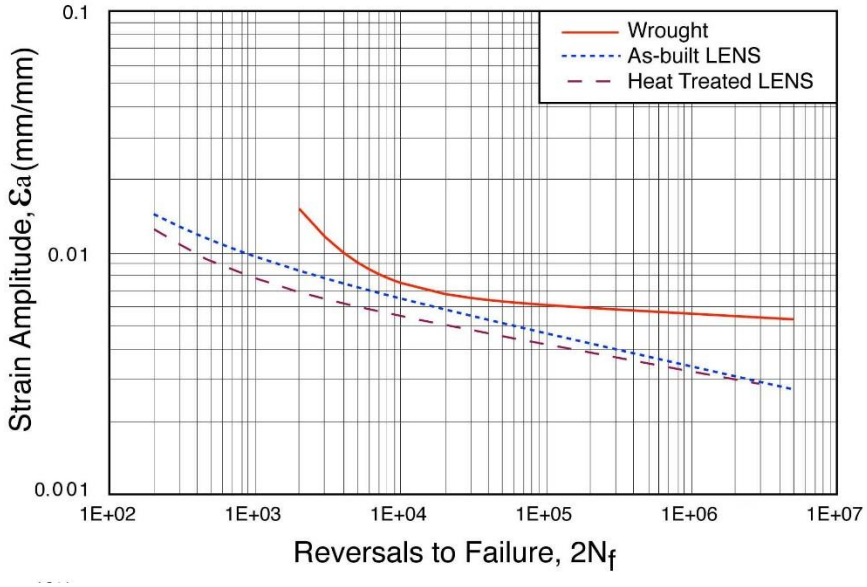

Figure 1. Ti-6Al-4V wrought, as-built LENS, and heat treated LENS strain-life fatigue curves generated using Coffin-Manson approach [6].

For homogeneous materials with isotropic microstructural features, applied loading produces a specific stress contour. The highest point in this contour becomes the critical failure point, and fatigue life can be predicted with some accuracy using this data. However, anisotropic AM parts with porous features will have a different fatigue resistance, with critical failure locations that may or may not correspond to the maximum stress. This clearly motivates a fatigue model that accounts for not only stress effects, but also microstructure (i.e., material resistance).

In this study, a microstructure-based Multi-Stage Fatigue (MSF) model, developed by McDowell et al. [7] for cast A356-T6 aluminum alloy, is calibrated for LENS fabricated Ti-6Al-4V samples and used to predict the range of strain-life behavior. This MSF model has been successfully applied to a number of materials, including A356-T6 Al alloy [7, 8], A380-F Al alloy [8], Acrylonitrile Butadiene Styrene (ABS) [9], and LENS AISI 316L stainless steel [10]. The model spans both high cycle fatigue (HCF) and low cycle fatigue (LCF), and predicts crack incubation, short crack growth, and long crack growth stages of fatigue failure.

In order to calibrate the MSF model, fatigue specimens were machined from LENS fabricated Ti-6Al-4V rods and either heat treated or left ‘as-built’. Fully-reversed strain-controlled fatigue tests (of varying amplitudes) were then conducted on the specimens, and a fractography investigation was performed on the fracture surfaces in order to determine crack initiation points and the shape of any pores or inclusions involved during fatigue failure. This information was then used to calibrate the MSF model for both data sets. The prediction results of the MSF model are compared with experimental data. Finally, some conclusions are made based on analyses performed in this study.

Experimental Setup

Specimens were fabricated as cylindrical rods (101.6 mm tall, Ø = 10.92 mm) using an Optomec LENS^{TM} 750 equipped with a 1 kW Nd:YAG laser. For the LENS process, a deposition head with multiple nozzles is used for blown-powder deposition in an inert atmosphere [11]. First, the laser is used to create a melt pool on a substrate into which metal powder is sprayed to form a molten bead. The deposition head then travels along a user-defined tool path, depositing material to form a solid layer (as the molten bead solidifies). Finally, the deposition head is incrementally raised, and the process is repeated to form subsequent layers and eventually create a final part or assembly.

Traditionally, the LENS process employs parameters (e.g. laser power, travel speed, powder feed rate, etc.) that are time-invariant. For such 'uncontrolled' LENS processes, the initial set of process parameters will greatly impact the final part quality – which is typically judged by density. In this particular study, the travel speed was set to 16.9 mm/s, the powder feed rate was set to 0.16 g/s, and the laser output power was set to 350 W.

The inert gas within the LENS chamber (typically argon) can be inadvertently introduced into the build structure in a number of ways, the most prominent being through poor selection of hatch spacing, i.e. the raster pattern dictating track deposits for filling in a layer. If tracks are spaced too far apart, more gas can become trapped during deposition of a subsequent layer. In this study, the hatch spacing and layer thickness were set to 0.51 mm. The track orientation was rotated by 90º after depositing each layer, causing each layer's deposition direction to be perpendicular to the previous one.

Twenty-four cylindrical specimens were fabricated one at a time (six per substrate); fifteen were left in the as-built state, while nine were heat treated at 1050 °C for two hours in argon atmosphere, then furnace cooled to room temperature. This specific heat treatment brings the samples above the beta transus temperature and allows time for grain growth, ensuring that the microstructure will be different than that of the as-built. One sample from each set was used to analyze the resulting microstructure. For the microstructural analysis, both transverse and cross-sectional areas were taken from the sample, mounted, polished, and etched with a solution of 2% hydrofluoric acid and 98% deionized water. The samples were then examined using an Axiovert microscope.

Once the cylinders were created and the heat treatment of the nine cylinders was completed, fatigue specimens were machined into the classic dog-bone shape. The dimensions, which adhere to ASTM Standard E606, are shown in Figure 2 [12]. The gage sections of the fatigue specimens were polished along the loading axis with subsequently finer grits, creating as close to a mirror finish as possible. This step limits the effects of surface roughness on the fatigue test.

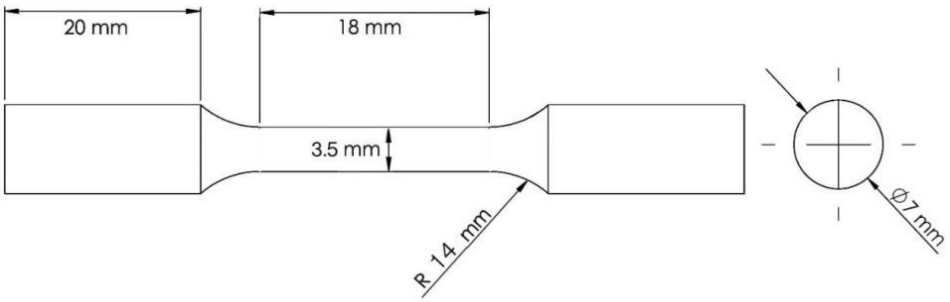

Figure 2. Dimensions of dog-bone cylindrical fatigue specimen

The density of each specimen was measured using Archimedes' principle. The volumetric displacement of water was found utilizing a standard graduated cylinder, and the weight was measured using a Denver Instrument APX-60 scale. The resulting calculated density of all the specimens of each type were then averaged together. This calculated density was subtracted from the ideal density for Ti-6Al-4V then divided by the ideal density, in order to find the percent porosity.

Fully-reversed uniaxial strain-controlled fatigue tests were performed using an MTS Tabletop 858 and an MTS Extensometer (Model 634.31F-25). To prevent the extensometer tines from scarring the surface of the gauge section, conservative amounts of epoxy (sanded to even heights) were used as a buffer. Once each specimen broke, a fractography investigation was conducted using a Scanning Electron Microscope (SEM). Crack initiation sites and final fracture zones were identified, along with any process defects (i.e. voids and inclusions) to be used for calibrating a microstructure-sensitive fatigue model.

Experimental Results

The microstructures of the as-built and heat treated LENS Ti-6Al-4V were compared with that of wrought Ti-6Al-4V as shown in Figure 3. In general, the wrought (Figure 3a) was predominately equiaxed, while the as-built LENS specimens (Figure 3b) demonstrated predominately columnar grain structure. The LENS as-built Ti-6Al-4V material experienced beta grain growth during the LENS process and alpha grain formation during cooling; it is clear that the wrought material did not share this experience. The heat treated LENS material (Figure 3c) displayed lamellar grains, due to it being brought above the beta transus and experiencing a longer cooling time during the heat treatment process.

Electron Backscatter Detection (EBSD) was used to determine the average grain size of the as-built LENS Ti-6Al-4V. The equipment was set to scan an area of 400 μm × 400 μm, with a step size of 0.5 μm and a voltage of 20 kV. The scan showed an average grain size of 32 μm (later used in the MSF model). This investigation also revealed that the material microstructure consisted of predominately alpha phase [6]. The density of each specimen was measured and the individual results were then averaged together for an overall 1.69% porosity for both the as-built and heat treated LENS fabricated Ti-6Al-4V.

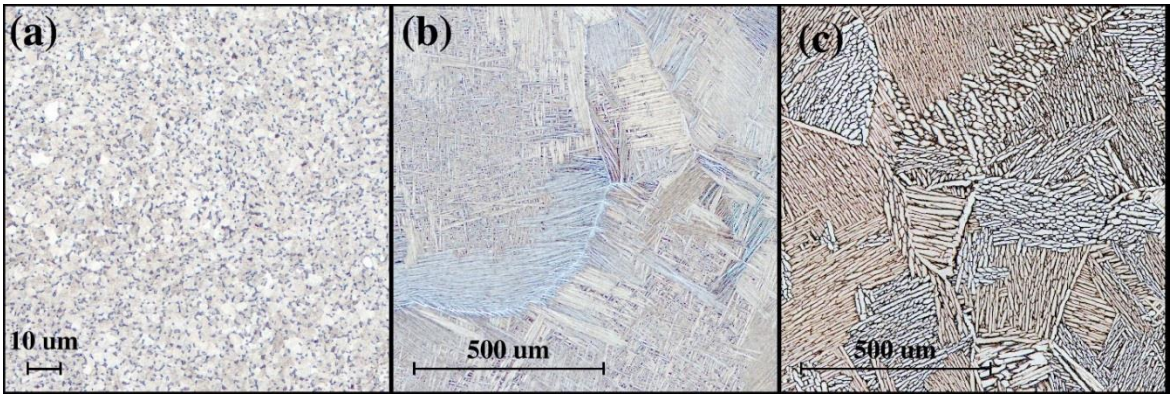

Figure 3. Cross-sectional microstructure comparison of (a) wrought, (b) as-built LENS, and (c) heat treated LENS Ti-6Al-4V.

During the fractography investigation, it was noted that the wrought material had a typical fracture surface, with clearly defined crack initiation, crack propagation, and final fracture regions. The fracture surfaces of the LENS materials, however, were significantly different, as shown in Figure 4. The as-built LENS surfaces had a mountainous terrain with multiple crack initiation points at pores, as shown in Figure 4a. The heat treated samples, with an example shown in Figure 4b, generally displayed less mountainous surfaces. Multiple crack initiation points were also present, but they were usually at the surface, not at pores. In fact, the heat treated LENS samples exhibited very little porosity on the fracture surface. The crack propagation seemed to correlate to the microstructure as the cracks followed a twisting, tortuous path during propagation, depending on the orientation of the lamellae in the alpha colonies. It was found that if the lamellae are somewhat parallel to the load axis, the crack cuts through the alpha colony, and if the lamellae are perpendicular to the load axis, the crack propagates along the alpha colony boundaries [6].

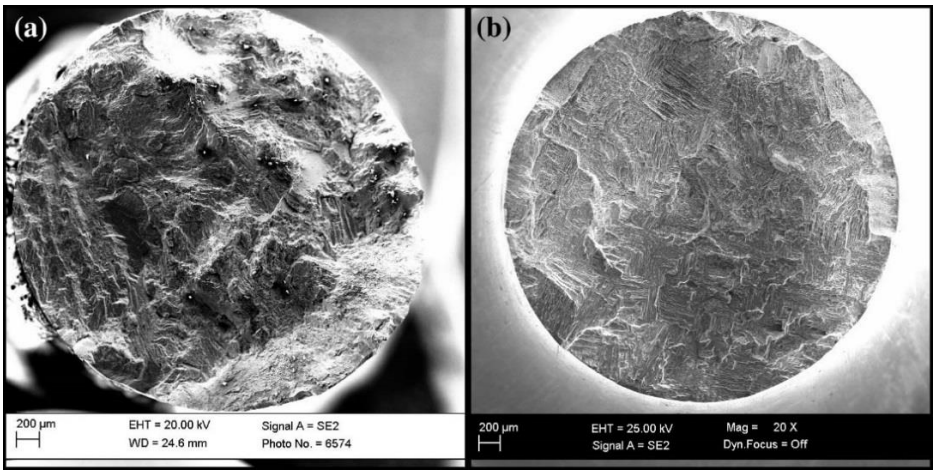

Figure 4. Representative fatigue fracture surfaces for (a) as-built LENS and (b) heat treated LENS Ti-6Al-4V.

Figure 5 presents a grayscale representation of the perceived fracture surface of the two samples in Figure 4. Neither sample exhibited noticeable long crack growth. There was little-to-no small crack growth in the as-built LENS sample, while the heat treated LENS sample exhibited a slight level of small crack growth. This is a prime example of different microstructures impacting

fatigue failure mechanisms; further justifying the need for calibrating a microstructure-sensitive fatigue model for AM parts.

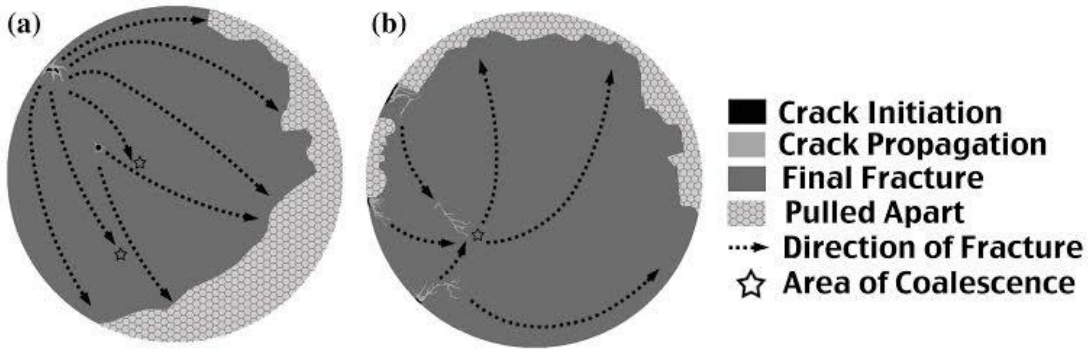

Figure 5. Grayscale representations of fracture history for (a) as-built LENS and (b) heat treated LENS Ti-6Al-4V fatigue specimens.

As previously shown in Figure 1, the resulting fatigue lives of the LENS specimens are much shorter than that of the wrought Ti-6Al-4V due, in part, to the microstructural differences. The LENS material was found to be much more brittle, which is detrimental in the short-life regimes. The shorter fatigue lives observed for LENS specimens are primarily attributed to process defects, which can also cause variation in fatigue lives, mostly in the long-life regime. Voids were observed to be the primary crack initiation sites for the as-built LENS fabricated Ti-6Al-4V. With this in mind, every void exposed on the fracture surface was quantified by size and location. A correlation was found between the void data and the variation seen in the individual fatigue test results (particularly noticeable in the long-life regime). The three parameters found to have the greatest effect on the fatigue lives were void size (the larger, the higher the impact), void location with respect to the free surface (the closer to the surface, the higher the impact), and the total number of voids (the more voids, the higher the impact). There were two other factors that played a less significant role, namely: void shape and the nearest-neighbor distance.

Fatigue Model Calibration

The Multi-Stage Fatigue (MSF) [7, 13] model is an example of a microstructure-sensitive fatigue model that considers various experimentally observed stages of fatigue damage evolution such as crack incubation, microstructurally small crack (MSC) growth, and long crack growth into account. The MSF model has been used to quantify the microstructural effects on fatigue life for many metallic alloys [13]. The unique feature of the MSF model is its ability to predict the observed variability in fatigue with respect to the variation of microstructural properties such as second phase particle size, grain size, pore size, texture, porosity, etc. The total fatigue life, N_{Total}, may be considered as [8-10]:

$$N_{Total} = N_{Inc} + N_{MSC} + N_{LC} \quad (1)$$

where N_{Inc} is the number of cycles to incubate a crack at a micro-notch formed by an inclusion, which can be a particle, or a pore. The incubated crack extends from the inclusion and propagates through a region which is still under influence of the micronotch. N_{MSC} is the number of cycles

required for growth of a microstructurally small crack. N_{LC} is the number of cycles required for long crack (LC) growth to final failure, which depends on the amplitude of loading and the extent of local plasticity ahead of the crack tip. For LENS Ti-6Al-4V specimens in this study, N_{LC} was not observed and was excluded from formulation [6].

Crack incubation at pores or inclusions is modeled using a modified Coffin-Manson relation and is split into two stages: crack nucleation and crack propagation within the influence of the micro-notch root field [7], as presented by Equation 2.

$$C_{INC} N_{INC}^{\alpha} = \beta \tag{2}$$

The linear and exponential material constants, C_{INC} and α, respectively, are selected to match those of the macroscopic Coffin-Manson and β is the nonlocal damage parameter based on the ratio between plastic zone size around a defect and the diameter of the defect, l/D [10]. Depending on the ratio, either Equation 3a or 3b will be used.

$$\beta = \frac{\Delta\gamma_{max}^{P*}}{2} = Y[\varepsilon_a - \varepsilon_{th}]^q, \frac{l}{D} < \eta_{lim} \tag{3a}$$

$$\beta = \frac{\Delta\gamma_{max}^{P*}}{2} = Y\left(1 + \zeta\frac{l}{D}\right)[\varepsilon_a - \varepsilon_{th}]^q, \frac{l}{D} > \eta_{lim} \tag{3b}$$

Parameters ε_{th}, ε_{per}, η_{lim}, r, and q all describe the ratio between the defect size and the plastic zone with respect to the strain amplitude, ε_a. Note that Y is a correlation defined by Equation 4, with R representing the load ratio, and y_1 and y_2 being constants, i.e.:

$$Y = y_1 + (1 + R)y_2 \tag{4}$$

When R = -1, as is the case in this study, $Y = y_1$. The l/D ratio is found using the non-local plastic shear strain and remote loading strain amplitude.

$$\frac{l}{D} = \frac{\langle\varepsilon_a + \varepsilon_{th}\rangle}{\varepsilon_{per} + \varepsilon_{th}}, \frac{l}{D} \ll \eta_{lim} \tag{5a}$$

$$\frac{l}{D} = 1 - (1 - \eta_{lim})\left(\frac{\varepsilon_{per}}{\varepsilon_a}\right)^r, \frac{l}{D} > \eta_{lim} \tag{5b}$$

As shown in Equations 6-7, during the MSC stage, crack growth is dependent upon the crack tip displacement range, ΔCTD. This range is proportional to crack length (a), the n^{th} power of the applied stress amplitude (σ_a^n) in the HCF regime, and the range of macroscopic plastic shear strain in the LCF regime. Note that χ is a material constant and ΔCTD_{th} is the crack tip displacement threshold. The CTD is a function of material dependent parameters (C_I, C_{II}, and ζ) and the remote loading [10].

$$\left(\frac{da}{dN}\right)_{MSC} = \chi(\Delta CTD - \Delta CTD_{th}), \quad a_i = 0.625D \tag{6}$$

$$\Delta CTD = C_{II}\left(\frac{GS}{GS_0}\right)^{\omega}\left(\frac{GO}{GO_0}\right)^{\xi}\left[\frac{U\Delta\hat{\sigma}}{S_{UT}}\right]^{\zeta} a_i + C_I\left(\frac{GS}{GS_0}\right)^{\omega'}\left(\frac{GO}{GO_0}\right)^{\xi'}\left(\frac{\Delta\gamma^P_{max}}{2}\right)^2 \quad (7)$$

The results of the MSF models are shown in Figure 6. The predicted fatigue life from the MSF model for the as-built LENS material (Figure 6a) showed agreement with the experimental data. Upper and lower bounds were generated using the smallest and largest average void diameter observed, approximately 10 μm and 90 μm, respectively. The upper bound fits the data satisfactorily, while the lower bound has too much variation for an exceptional fit, due to the largest average pore size being an outlier. Due to the test being stopped once it passed 1,000,000 cycles, as a runout, the data point is outside the lower bound. The MSF model for the heat treated LENS material (Figure 6b) fit the data fairly well. The upper and lower bounds fit closer for the heat treated LENS Ti-6Al-4V, due to less variation in void diameter observed on the fracture surface. These bounds were created using void diameters of 19 μm and 48 μm. The bounds in the MSF model give a range of possible fatigue lives depending on the microstructural properties and defects.

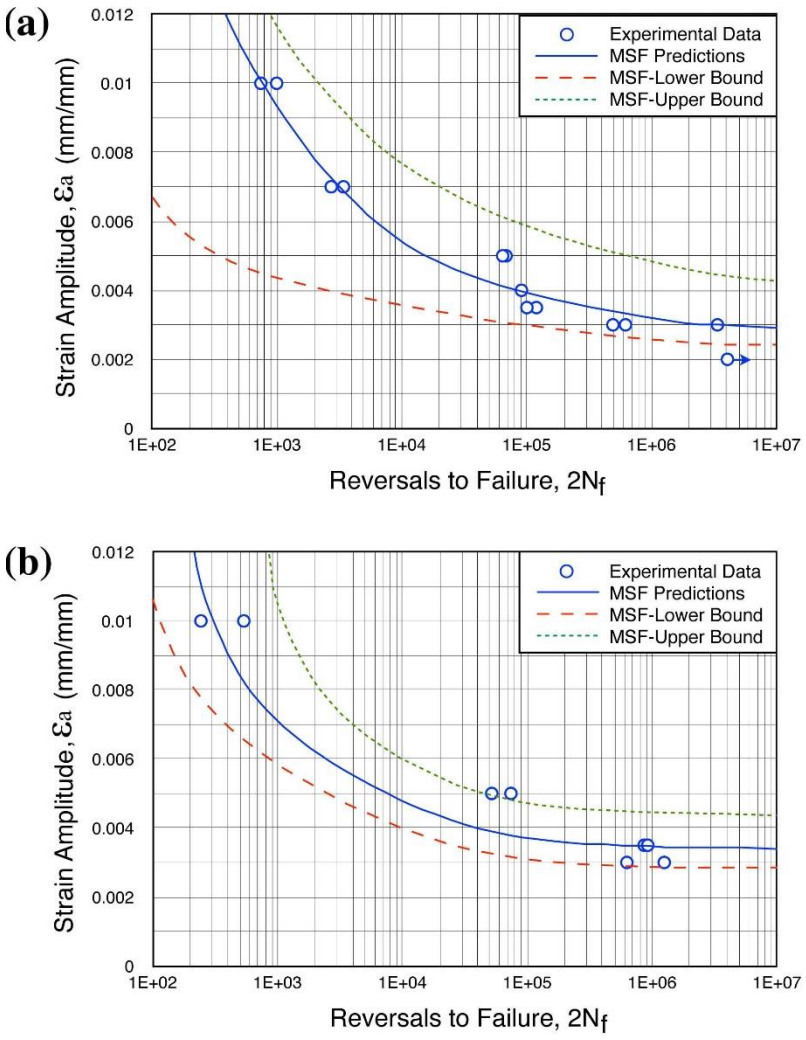

Figure 6. Fatigue life predictions using MSF model for (a) LENS as-built and (b) LENS heat treated Ti-6Al-4V. Upper and lower prediction bounds obtained for largest and smallest incubation voids are also presented.

The LENS as-built material had much wider bounds than the heat treated LENS material. This is due to a limited number of unusually large pores observed on the fracture surface. For the LENS as-built material, the outlier sizes occurred at 0.35% and 1.00% strain amplitudes, causing the bound to shift to the left. As the pivoting point appeared to be around 0.35%, the large, irregularly shaped pores located at the free surface of the fatigue specimens caused a drastic shift in the lower bound. The heat treated LENS material had a closer fit. This is attributed to the failure of the material not being driven by the pores. There were significantly fewer voids found on the fracture surfaces, despite the overall part porosity being comparable to the LENS as-built material. This shows that voids can influence the scatter in the data if the failure is driven by voids; hence, as more control is gained over the LENS process, the tighter the bounds will become in the MSF model. A better-controlled LENS process would not only limit the porosity, but also allow for more uniform void sizes and shapes in the remaining porosity.

Conclusions

This study quantified the defects and microstructural properties driving the fatigue behavior of as-built and heat treated LENS fabricated Ti-6Al-4V. As the uncontrolled LENS manufacturing process typically involves non-uniform thermal histories, the process may produce different microstructures throughout the part. Different microstructures beget different local fatigue resistances throughout the build, thereby making it difficult to predict fatigue life using methods traditionally applied to homogenous/isotropic materials. This demonstrates the need for a microstructure-sensitive fatigue model for use with AM fabricated material. Hence, a microstructure-sensitive fatigue model was used to predict the strain-life behavior of the materials, while taking into account the uncertainty caused by process defects such as voids and inclusions. In particular, the following conclusions can be made:

1. The Ti-6Al-4V, in either the as-built or heat treated condition, had a shorter fatigue life than that of the wrought Ti-6Al-4V material.

2. Both LENS materials had different microstructures than the wrought Ti-6Al-4V.

3. Fractography into the as-built LENS material showed that, unlike the heat treated LENS material, voids were primarily responsible for the incubation regime during fatigue and that small crack growth was very limited. In the heat treated LENS fabricated samples, the incubation did not occur at pores, but began on the surface near the grain boundaries. Small crack growth was limited, though not to the extent seen in the as-built samples.

4. Satisfactory fatigue life predictions were obtained using the microstructure-sensitive MSF model for both as-built and heat treated LENS Ti-6Al-4V.

5. Wider bounds in the MSF model were seen for the as-built LENS material due to the larger range of pore sizes, begotten from the infrequent occurrence of unusually large voids.

6. The lower bound of the as-built LENS material seemed to pivot due to the pore size outliers. There was no noticeable pivot in the lower bound of the heat treated LENS material, likely due to the limited impact the voids had on the fatigue failure.

7. The heat treated LENS fabricated material had tighter bounds in the MSF model. This is largely due to smaller deviation in pore size and the lesser role porosity played in the failure of the fatigue specimens.

References

[1] Sterling, A.J., Shamsaei, N., Torries, B., Thompson, S. M., "Fatigue Behaviour of Additively Manufactured Ti-6Al-4V," International Conference on Fatigue Design, Senlis, France, 2015.

[2] Brandl, E., Leyens, C., Palm, F. "Mechanical Properties of Additive Manufactured Ti-6Al-4V using Wire and Powder Based Processes," Trends in Aerospace Manufacturing 2009 International Conference, TRAM09, IOP Conference Series: Materials Science and Engineering 26, 2011.

[3] Wu, Xinhua, et al, "Microstructures of Laser-deposited Ti-6Al-4V,"Materials and Design, Vol. 25, No. 2, 2014, pp. 137-144.

[4] Mutombo, K, 2013, "Metallurgical Evaluation of Laser Additive Manufactured Ti6Al4V Components" Rapid Product Development Association of South Africa (RAPDASA) conference, SanParks Golden Gate Hotel, South Africa.

[5] Selcuk, C., "Laser Metal Deposition for Powder Metallurgy Parts," Powder Metallurgy, Vol 54, Issue 2, 2011, pp. 94-99.

[6] Sterling, A. J., Torries, B., Shamsaei, N., Thompson, S. M., and Seely, D., "Fatigue Behavior and Failure Mechanisms of Direct Laser Deposited Ti-6Al-4V," submitted.

[7] McDowell, D.L., Gall, K., Horstemeyer, M.F., Fan, J., "Microstructure-based Fatigue Modeling of Cast A356-T6 Alloy," *Engineering Fracture Mechanics*, Vol. 70, 2003, pp. 49-80.

[8] Xue, Y., Burton, C.L., Horstemeyer, M.F., McDowell, D.L., and Berry, J.T., "Multistage Fatigue Modeling of Cast A356-T6 and A380-F Aluminum Alloys," *Metallurgical and Materials Transactions B,*Vol. 38B, 2007, pp. 601-606.

[9] Lugo, M., Fountain, J. E., Hughes, J.M., Bouvard, J., and Horstemeyer, M.F., "Microstructure-Based Fatigue Modeling of an Acrylonitrile Butadiene Styrene (ABS) Copolymer," *Journal of Applied Polymer Science*, 2014, pp. 1-12.

[10] Xue, Y., Pascu, A., Horstemeyer, M.F., Wang, L., and Wang, P.T., "Microporosity Effects on Cyclic Plasticity and Fatigue LENS^{TM}-Processed Steel," *Acta Materialia*, Vol. 58, 2010, pp. 4029-4038.

[11] Griffith, M.L., Keicher, C.L., amd Atwood, C.L., "Free Form Fabrication of Metallic Components Using Laser Engineered Net Shaping (LENS^{TM})," Solid Free Form Fabrication Symposium, Austin, Texas, USA, 1996.

[12] ASTM E606 / E606M-12, Standard Test Method for Strain-Controlled Fatigue Testing, ASTM International, West Conshohocken, PA, 2012, www.astm.org

[13] Horstemeyer, M.F., Integrated Computational Materials Engineering (ICME) for Metals: Reinvigorating Engineering Design with Science, Wiley Press, 2012.